Engineering Research Express

PAPER

Analysis of a passive vibration damper for high-speed superconducting magnetic bearings

M Baloochi[1,*], T Espenhahn[1], M Hossain[2], Y Perez-Delgado[3], A Abdkader[2], M Beitelschmidt[3], K Nielsch[1] and R Hühne[1]

[1] Leibniz Institute for Solid State and Materials Research, Helmholtzstrasse 20, 01069 Dresden, Germany
[2] Institute of Textile Machinery and High Performance Material Technology (ITM), Faculty of Mechanical Science and Engineering, TUD Dresden University of Technology, Dresden, Germany
[3] Faculty of Mechanical Engineering, Technische Universität Dresden, Institute of Solid Mechanics (IFKM), Chair for Dynamics and mechanism Design, Marschnerstr. 30, 01307 Dresden, Germany
[*] Author to whom any correspondence should be addressed.

E-mail: armanbaloochi@gmail.com **and** m.baloochi@ifw-dresden.de

Keywords: superconducting magnetic bearing, eddy current damper, high-speed rotation, numeric modeling, vibration analysis, ring spinning

OPEN ACCESS

RECEIVED
6 May 2024

REVISED
19 June 2024

ACCEPTED FOR PUBLICATION
2 July 2024

PUBLISHED
25 July 2024

Abstract

Superconducting magnetic bearings (SMB) based on a combination of high temperature superconductors and permanent magnets enable the realization of self-stabilized high-speed devices with significantly reduced friction. However, external vibration might couple in the bearing resulting in large amplitude oscillations due to a resonance case. A dedicated eddy current damper (ECD) might be used to eliminate these oscillations for a stable operation. The influence of such damping elements was studied for a frictionless SMB twisting system designed to speed up the conventional ring spinning process. Therefore, conductive copper rings with different thicknesses were implemented at different positions into the bearing setup as ECD. Afterward, the SMB setup was analyzed during acceleration using an array of laser distance sensors to record the displacement of the levitating permanent magnet ring in radial and axial direction, respectively. Simultaneously, a numerical model was developed to investigate the influence of the ECDs on the dynamic and static behavior of the SMB in more detail. It was shown that the simulated damping coefficients are in good agreement with the measured values, which allows further optimization of the ECD with the developed numerical model.

1. Introduction

Superconducting magnetic bearings (SMB) are based on a combination of high-temperature superconductors (HTS) with permanent magnetic materials and show the unique characteristic of stable frictionless levitation [1]. This levitation is characterized by self-stabilizing suspension forces in all directions in contrast to pure magnetic or electromagnetic suspension systems, which require a complicated arrangement of permanent magnets or an active control system. In general, the restoring forces in the SMB between the permanent magnet (PM) and the superconductor originate from the so-called flux pinning effect, which 'freezes in' a magnetic field configuration during field cooling of the HTS material. As a result, each relative movement of the superconductor in the inhomogeneous magnetic field of the PM leads to restoring forces to maintain the cooling position. However, force-free movements are possible if the magnetic field configuration inside the superconductor is not changed. This is used for rotational bearings, where the field remains unaltered along a PM ring. Therefore, only an extremely low rotational drag is required for a rotation of the HTS in the field of the ring (or vice versa), which makes such SMBs a suitable choice for the design of rotating devices [2, 3]. Previously, such SMBs were tested for various applications such as flywheels [4–7], cryogenic pumps [8, 9] or motors [10]. More details with a focus on flywheel applications are found in a recent review [1].

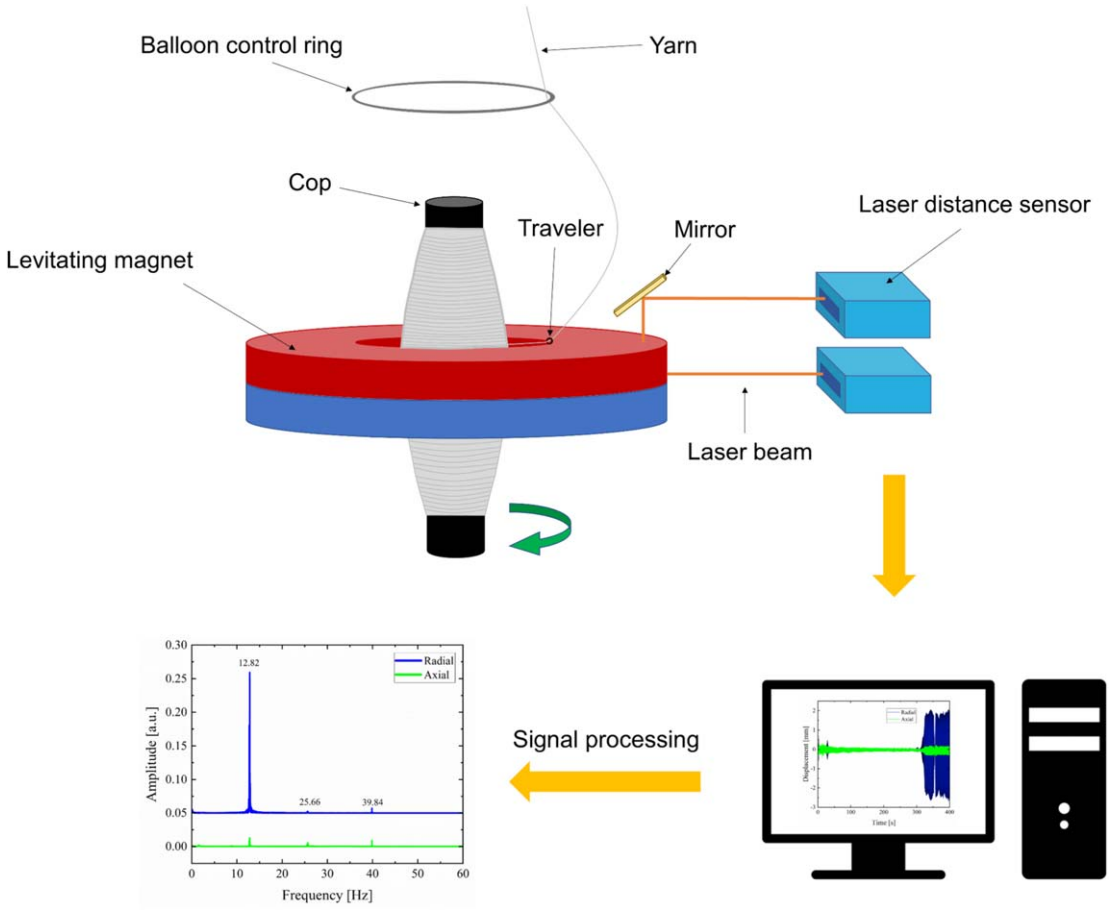

Figure 1. Basic concept for the analysis of the ring spinning process. The levitating magnet displacement was recorded with laser distance sensors in axial and radial direction. The measured signals are processes afterwards using an FFT algorithm.

In the last decade, our groups focused on designing, characterizing, and optimizing such a high-speed SMB for a ring spinning process in textile industry to produce the best quality of ring spun yarn in short staple yarn production [11–15]. The main goal of these efforts is to increase the speed of the ring spinning process to 50,000 RPM, which is about twice the maximum value used in conventional ring spinning. The mechanism of the ring spinning process and the setup of the SMB system are discussed in detail in previous publications [12, 15]. Figure 1 shows the basic concept of the ring spinning process and of the measurement setup. The movement of the levitating magnet is recorded during the acceleration and spinning process with laser distance sensors. The resulting data are analyzed to reveal the main oscillation frequencies of the system. In general, a reinforced PM ring is freely rotating above a superconducting ring, which is placed inside a cryostat. The schematic setup of the bearing itself is shown in figure 2. Originally, none of the shown copper rings were installed in the bearing. A stable rotation is observed during the dynamic acceleration of the PM ring up to speeds above 10,000 RPM. However, for higher speeds, additional fast radial oscillations of the PM ring were frequently observed with amplitudes of up to 2 mm depending on parameters as cooling height, yarn quality, or acceleration sequence [14]. A detailed analysis clarified that such oscillations most probably originate from a resonance case, where the natural frequency of the bearing gets close to one of the vibration frequencies of the surrounding machine exciting the bearing itself. Such oscillations of the PM ring significantly influence the yarn quality and frequently result in yarn breakage, severely disturbing the process flow. Therefore, appropriate measures must be taken to avoid or reduce such additional oscillations.

Although field-cooled SMB setups show a stable levitation, the bearing itself is relatively soft, i.e., small movements of the PM relative to the superconductor are possible with a strong dependence on the used magnetic field distribution and cooling height. In the dynamic case, this behavior is described with the bearing's stiffness and damping coefficient [16]. Depending on these values, the bearing might become dynamically unstable, resulting in extreme resonance cases. In these situations, oscillations with large amplitudes occur, which might cause malfunction or failure in the rotating device or the operating process. Therefore, designing a damping element that reduces or even eliminates these oscillations is of great importance. In some approaches, additional active magnetic bearings (AMB) are used in a hybrid setup to stabilize the SMB [17–20]. One example

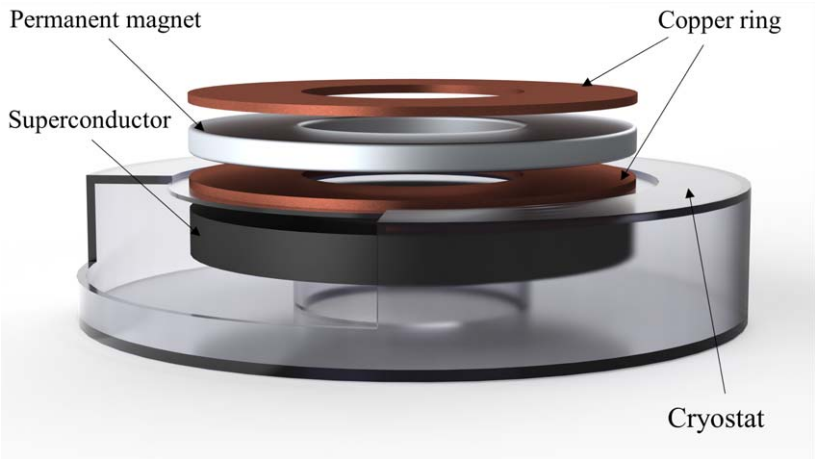

Figure 2. Schematic drawing of the used SMB setup with a freely levitating magnet ring and the position of additional copper rings as damping elements.

is an SMB system for flywheel applications, which is mainly controlled actively to eliminate radial oscillations of the rotor [19, 20]. Secondly, the concept of an electromagnetic shunt damper was tested to reduce axial oscillations in a SMB setup [21–23]. Such a passive system consists of a specially designed coil placed above the PM, which is connected to a shunt circuit with a resistor and a capacitor. Another method to reduce the detrimental oscillations significantly is to use eddy current dampers (ECD). They are simple, effective, and cheaper than active elements, for which external devices typically need to be added in experimental setups [24]. Since the eddy currents produce a repulsive force proportional to the velocity of the magnetic bearing, it behaves as a viscous damper. Eddy current dampers are used in a variety of industrial and technological fields, such as civil structures to prevent earthquake and strong wind damage [25], automobile suspension [26], vibration suppression of a beam or a cantilever [27, 28], and mitigating multi-mode cable vibration [29]. ECDs were already studied in combination with SMB setups to maintain stable levitation. For example, Jiang *et al* numerically investigated the effect of additional conducting elements on the damping of vertical vibrations inside a simple SMB setup consisting of a parallel-aligned superconducting and magnetic disk [30]. Furthermore, Jin *et al* studied the effect of an ECD on the dynamic behavior of a linear levitating maglev system when subjected to external disturbances such as cross-wind or track irregularities [31]. Finally, Detoni *et al* evaluated the damping characteristics for a radial permanent magnetic bearing with additional ECD elements by finite element simulations and experimental studies [32].

We aim to study the influence of such ECD elements on an existing SMB setup used for ring spinning studies at high speeds numerically and experimentally. Therefore, we added additional conducting Cu rings to the bearing, as illustrated in figure 2. In a first step, the PM ring's magnetic field was measured to develop and validate a numerical model for this field using COMSOL MULTIPHYSICS 5.6. These data were used for a 3D numerical model of the SMB to study the dynamic behavior for different arrangements of eddy current damper around the PM ring. In a second step, the bearing was characterized in a static and dynamic mode to verify the influence of selected ECD arrangements. This will allow us to optimize the ECD further for our application scenario.

2. Basic investigations on the SMB setup

Figure 2 illustrates the schematic setup of the SMB with integrated conductive Cu rings. For this study, we used the following steps to initialize the bearing. The PM ring was placed by spacers at 4.5 mm distance to the upper edge of the superconductor ring, which consists of $YBa_2Cu_3O_{7-x}$ (YBCO) segments. Afterward, liquid nitrogen cools the superconductor to 77 K inside the cryostat. Finally, the spacers were removed so that the PM is freely levitating above the superconductor. At this stage, the PM moves about 0.1 mm towards the superconductor due to its weight, i.e. the final working distance between PM and superconductor is about 4.4 mm. It should be noticed that the gap between the cryostat wall above the superconductor and the PM ring is just about 1.5 mm, limiting the thickness of the lower copper ring. In a first step, the behavior of the SMB was characterized by different methods without any Cu ring. Afterward, Cu rings with different thicknesses were placed on top of the cryostat between the superconductor and the PM to study the influence of the eddy current dampers on the behavior of the SMB. For a second set of experiments, a 1 mm thick Cu ring having a larger outer diameter was

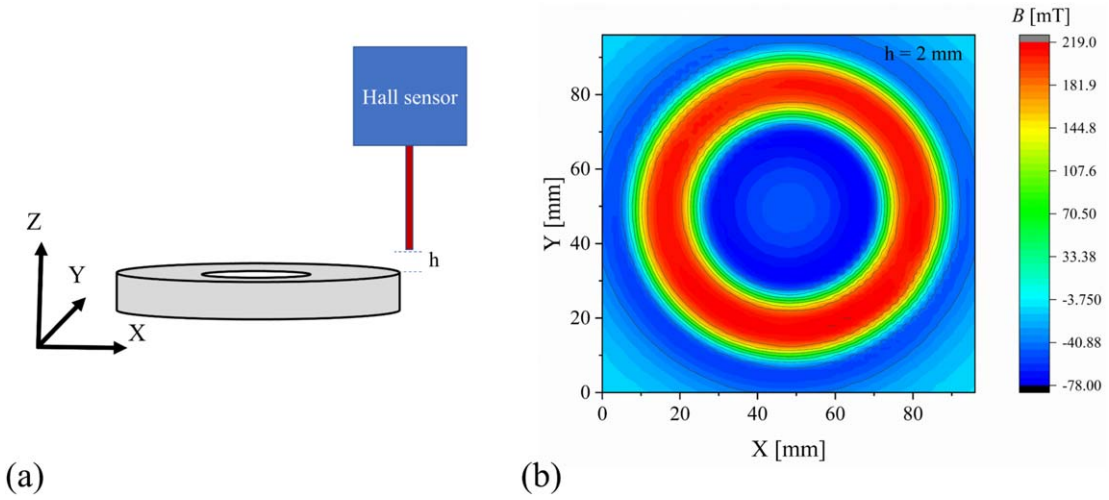

Figure 3. Characterization of the magnetic flux distribution for the used PM ring, (a) schematic illustration of Hall probe measurement setup (h: measuring height), (b) Contour plot of the magnetic field distribution 2 mm above the PM ring.

fixed on the upper surface of the cryostat below the PM. This allowed to place additional copper rings above the PM, which are mechanically connected to the lower copper ring by threated rods and nuts.

2.1. Magnetic field distribution of the PM ring

A ring-shaped NdFeB permanent magnet (grade N40SH) with an outer diameter of 80 mm, an inner diameter of 50 mm, and a thickness of 6 mm is used for this study. During operation at high rotational speed, the centrifugal force on the sintered PM ring might result in a crack formation and, finally, in a breaking of the magnet. To avoid this, the PM ring was reinforced by an outer shell from a non-magnetic high-strength Ni alloy (Alloy 718) with an outer diameter of 100 mm. More details are described in [14].

The magnetic field distribution of the axially magnetized PM ring was scanned at different heights ($h = 1$–8 mm) above the surface with a Hall sensor (MCA-2560-WN-03) attached to a stepper motor-controlled X-Y table (compare figure 3(a)). The used step size for the measurement in X and Y direction was 2 mm. The Hall sensor was sensitive to the magnetic flux density in Z direction, i.e., only the magnetic field's B_z component was determined. The results in figure 3(b) show a homogeneous distribution of the magnetic field along the circumference, which is essential for a lossless operation of the superconducting magnetic bearing. Figure 4 summarizes the measured maximum magnetic flux density for different distances between the Hall sensor and the top surface of the PM.

2.2. Numerical model for the flux distribution

A numerical model was created for the magnetic field of the PM ring to simulate the influence of the damping elements on the behavior of the SMB. Since the measurement results in section 2.1 showed a homogenous distribution of magnetic flux density along the circumference of the magnet ring, we only consider the cross-section of the PM ring to build the numerical 2D model, which is easier to handle and more time efficient. Therefore, a numerical model based on the finite element method was set up in COMSOL MULTIPHYSIC 5.6 using Maxwell's equations. In this numerical model the equations were solved by the stationary solver of COMSOL. In general, the used simulation domain consists of the PM and surrounding air only. The boundaries of air domain were set to magnetic insulation condition. A linear dependence of the magnetization on the magnetic field is expected as the magnet is kept at room temperature. Afterwards, a parametric study was performed, where the remanent flux density B_r was fitted to the measured flux density at different heights as shown in figure 4. The optimized B_r will be later imported to the 3D model of the eddy current damper.

2.3. Static force measurement of the bearing

For this study, the permanent magnet ring was placed at a distance of 4.5 mm from the surface of YBCO during field cooling. The interaction force between the levitating PM ring and the superconductor was measured with a 3-axis force sensor setup (Model number: FTD-Mini-45 SI-580-20), where the magnet was fixed to the sensor itself, and the cryostat, including the superconducting ring, was moved by stepper motors in radial direction. The step motor velocity was set at 1 mm s^{-1} for all measurements. The experimental procedure is sketched in the inset of figure 5. Therefore, the PM ring was moved ± 2 mm out of the cooling position in radial direction

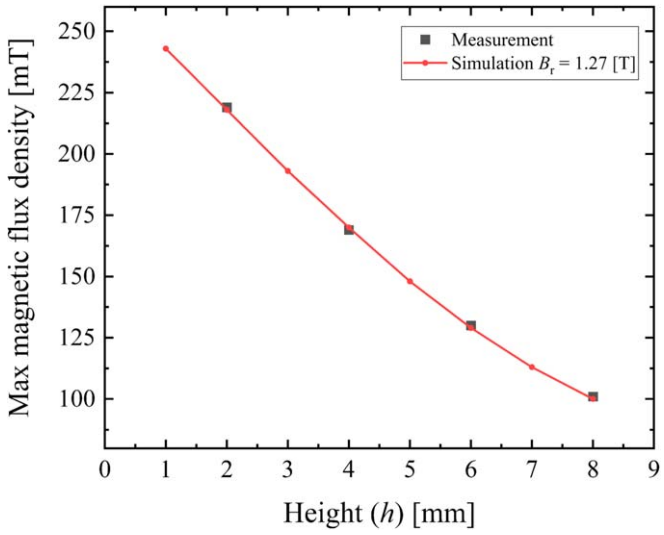

Figure 4. Maximum flux density at different heights above the used PM ring. The numerical model of the magnetic flux density uses the remnant flux density B_r as fitting parameter.

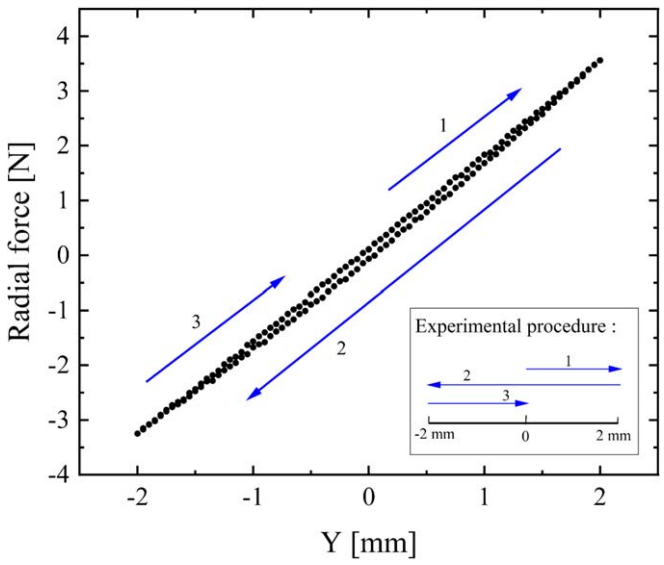

Figure 5. Measurement of the radial restoring force for the SMB (cooling height: 4.5 mm, T = 77 K).

recording the restoring force. It should be noted that this displacement is comparable to the maximal amplitude of the PM oscillations observed in our SMB setup (compare figure 7). The results in figure 5 indicate that the restoring force exhibits an almost linear behavior with a very small hysteresis loop. The linear fit of the slope gives a value of about 1700 N/m for the radial static stiffness of the bearing for small displacements.

2.4. Modelling of the dynamic behavior

As the restoring force shows an almost linear dependence for radial displacements of the PM up to 2 mm (figure 5), we will neglect the effect of a non-linear behavior for the numerical study of SMB oscillations. Consequently, the levitating PM ring can be represented by a simple mass-spring-damper model, as shown in figure 6(a). The motion equation that holds for such a model is:

$$m \quad \ddot{x} + C_{SMB} \quad \dot{x} + K_{SMB} x = f(t) \tag{1}$$

Here, m is the mass of the PM, which is 0.25 kg in our case. C_{SMB} in [N.s/m] and K_{SMB} in [N/m] are the damping coefficient and the spring constant or dynamic stiffness of the SMB, respectively, $f(t)$ is the external force in [N] applied on the PM, and x in [m] is the displacement in radial direction. Adding the Cu rings as external eddy current dampers will give an additional damping coefficient C_{ECD} in [N.s/m], which leads to the

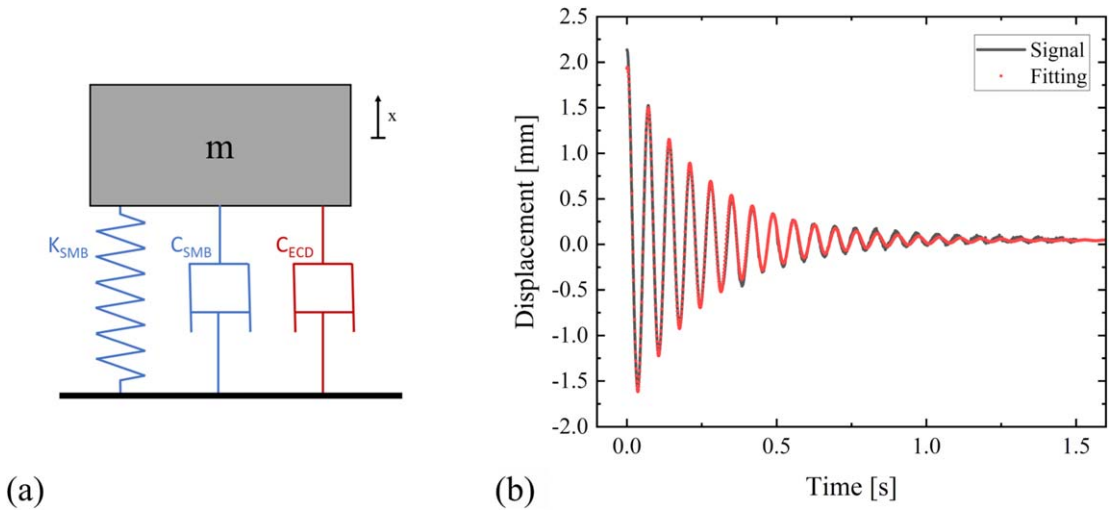

Figure 6. (a) Schematic setup of the mass-spring-damper model, (b) Exemplary measured response signal of a radial impulse excitation with the result of the fitting giving a natural frequency $\omega_n = 81.24$ rad s^{-1}, a damping ratio $\zeta = 0.044$, a damping coefficient $C_{SMB} = 1.79$ N.s/m and a dynamic stiffness $K_{SMB} = 1656$ N m^{-1}.

following equation:

$$m \quad \ddot{x} + (C_{SMB} + C_{ECD}) \quad \dot{x} + K_{SMB} \quad x = f(t) \tag{2}$$

For basic investigations, the levitating magnet of the SMB was deflected by an impulse using a hammer with a titanium tip. The movement of the magnet in radial direction was recorded by an array of optical laser sensors (more details are given in the following section as well as in [12]). The system's response to the impulse signal is shown in figure 6(b) for an exemplary case. Afterward, the measured displacement curves were fitted with the general solution of the motion equation for an underdamped free vibration:

$$x(t) = A \quad e^{-\zeta\omega_n t} \sin(\omega_d \quad t + \phi_d) \tag{3}$$

$$\omega_d = \omega_n \sqrt{1 - \zeta^2} \tag{4}$$

ζ is the dimensionless damping ratio, ω_n in [rad/s] and ω_d in [rad/s] are the system's natural undamped and damped frequency, t in [s] the time, and $\varnothing_d$ the signal's phase. The damping ratio is given as:

$$\zeta = \frac{C_{eq}}{2\sqrt{K_{eq} M_{eq}}} \tag{5}$$

C_{eq} in [N.s/m], K_{eq} in [N/m] and M_{eq} in [kg] are the bearing's equivalent damping coefficient, stiffness, and mass, respectively.

2.5. Analysis of the SMB during the acceleration phase

The complete SMB setup is installed in a ring spinning tester as described in more detail previously [12, 33]. For the tests, fibers from 100% cotton with a yarn count of 20 tex (1 tex = 1 g km^{-1}) were used. Additionally, a yarn twist of 800 TPM (twist/meter) and a total draft of 26 were used. In the following, the behavior of the SMB was studied for the first time during the acceleration phase. The rotation speed of the spindle was increased within several intervals with a rate of 27.7 RPM/s (2.9 rad s^{-2}). The resulting spindle speed is plotted in the related figures. During the process, the yarn is moving through a clip attached to the PM ring and wound on the spindle. As a result, the yarn pulls on the levitating PM ring and accelerates it. The resulting speed of the PM is about 2% smaller compared to spindle speed [12]. In general, the yarn force pulls on the PM ring under an angle with a radial and an axial force component. However, the force value is typically below 200 cN [33, 34], i.e., only a minor displacement is expected. Additionally, vibrations from other moving parts of the ring spinning tester might couple in the SMB resulting in an excitation of the bearing as previously shown for the steady spinning case [12]. In the following, the behavior of the PM during acceleration will be studied in detail.

A set of 5 synchronized optical laser sensors is used to track the movement of PM during operation. More details on the setup of this sensor array are described in a previous publication [12]. The real-time signal during the acceleration phase obtained from two of the five distance sensors is shown in figure 7(a). At low rotational speeds, the oscillation amplitude in both axial and radial directions is small; therefore, so the ring spinning process is stable. However, for a specific rotation speed range, high amplitude oscillations arise, which are more severe in radial direction. This is plausible as the restoring forces between the superconductor and PM are

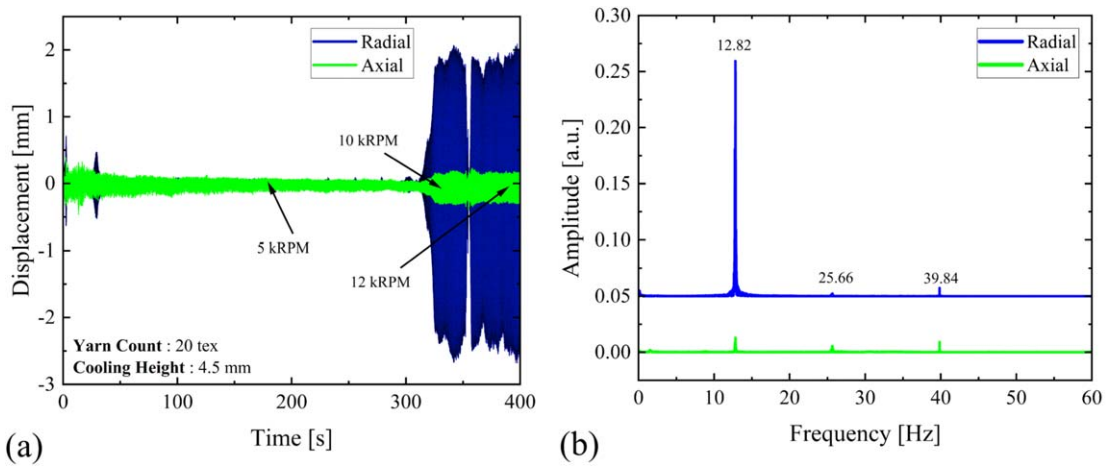

Figure 7. (a) Displacement of the PM ring in radial and axial direction during the acceleration phase of the ring-spinning process (the arrows show the PM ring speed during the acceleration phase) (b) Fast Fourier Transform (FFT) analysis of the displacement signals during the acceleration phase, a vertical offset of 0.05 was applied for the radial case for better visibility of the peaks.

smaller in radial compared to axial direction, i.e., the bearing shows the smallest stiffness when submitted to a radial force, resulting in larger oscillations. It should be mentioned additionally that the amplitude of these vibrations is larger compared to previous studies as a larger cooling distance (4.5 mm instead of 3 mm) as well as a higher temperature at the superconductor (77 K instead of 66 K) was used for the new measurements resulting in a lower stiffness of the SMB.

A Fast Fourier Transform (FFT) algorithm was performed on the signals to convert the data from the time domain to the frequency domain using MATLAB functions. The main peaks in the resulting frequency spectra were similar for the radial and axial cases. The peak with the highest intensity corresponds to the oscillation frequency of the bearing. It will be shown later that this frequency is close to natural/resonance frequency of the bearing in radial direction. Other peaks arise from higher orders of this harmonic oscillation. When the spindle speed reaches 12,000 RPM, the bearing enters a resonance region and starts oscillating at high amplitudes. In this region, the applied tension on the yarn might get larger than its mechanical strength eventually leading to yarn breakage, which will stop the ring spinning process. One approach toward solving this problem is to decrease the oscillation amplitude by increasing the damping coefficient of the bearing using eddy current dampers as shown in the following.

3. Influence of the eddy current dampers on the behavior of the SMB

In the following, we analyzed the influence of additional eddy current dampers on the dynamic behavior of the SMB. These elements have the advantage of not requiring an active control system with an external power supply or other electronic equipment. ECDs typically consist of a highly electrically conductive material. The alternating magnetic field of the moving PM ring induces eddy currents creating a magnetic field with opposite polarity to the initial magnetic flux. So, the coupling between the induced eddy current and the original magnetic field will generate a mechanical repulsive force between the conductor and the PM ring through the so-called Lorenz force, which is proportional to the velocity of the PM ring. As a result, this force will reduce the oscillation amplitude of the magnetic ring. At the same time, the induced eddy current inside the conductive material will generate heat, which is proportional to the electrical resistance of the conductive material and the induced eddy current density. To study the behavior of an ECD in detail, Cu rings (grade Cu-DHP (CW024A)) with different thicknesses are placed in the free space between the superconductor and the PM as well as above the PM ring. In the circumferential direction, the magnetic field of the PM is homogenous, i.e., no field change occurs when the PM rotates over the Cu plate. As a result, no eddy currents are induced in the copper ring if the PM rotates only.

3.1. Influence of ECD on the damping ratio of the SMB

As a first step, the influence of the ECD on the SMB properties was studied in a stationary mode using an impulse test similar to the investigation in section 2.4. The results of these studies allow us to optimize the damper configuration for the ring spinning process itself. Therefore, copper plates with different thicknesses were placed in the air gap between the cryostat and the PM ring. Afterwards, an impulse test was done ten times recording the position of the PM ring with the optical sensor array in radial direction. The oscillatory movement of the magnet

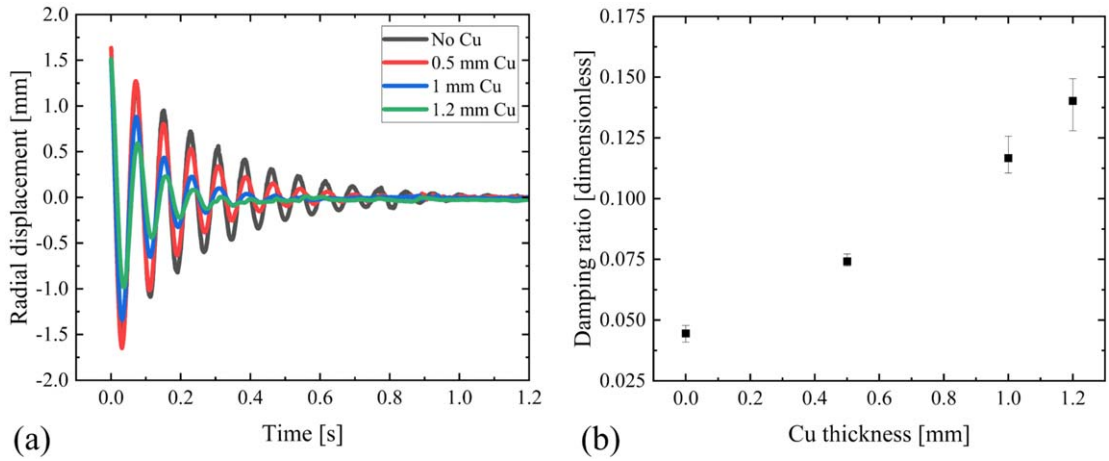

Figure 8. Effect of the thickness of a single Cu ring between the superconductor and the PM on: (a) the response signal to a single impulse in radial direction; (b) the damping ratio of the bearing.

is exemplarily shown in figure 8(a) for different Cu thicknesses. It clearly indicates how an increasing Cu thickness increases the damping of the system. The determined damping ratios ζ are summarized in figure 8(b) showing a clear correlation between damping and copper plate thickness. As a result, adding a 1 mm thick copper plate increases the damping by a factor of 2.6 compared with the original case. Therefore, these copper plates might ensure the stability of the magnetic bearing when large oscillations occur in a resonance case. However, the available space for the Cu plates in the air gap between the cryostat and the PM is restricted. In general, a small distance between the superconductor and the PM is desired to increase the stiffness of the bearing itself. Additionally, any mechanical contact between the PM and the Cu ring must be avoided for high rotational speeds to ensure a safe operation of the ring spinning process. To solve this problem, we will use an additional copper plate above the rotating PM ring (compare figure 2), which will help to increase the damping by increasing the total thickness of the conductive plate.

3.2. Estimation of damping in resonance

It was shown with the FFT analysis of the data from the laser distance sensors during the acceleration phase that the large amplitude oscillations in radial direction above 12,000 RPM have a frequency of 12.8 Hz. In contrast, other frequencies can be neglected (compare section 2.5). Previous studies on similar bearings indicated that the natural frequency of the bearing is in this range [14, 16]. We will describe our bearing as a single-frequency harmonic oscillator in radial direction as we observe just a single frequency. With this assumption, the magnification factor M, which is the transmitted force over the excitation force, can be written as:

$$M(r,\,\zeta) = \frac{1}{\sqrt{(1-r^2)^2 - (2\zeta r)^2}} \tag{6}$$

Where r is the ratio between the excitation frequency and the natural frequency of the bearing:

$$r = \frac{\omega}{\omega_n} \tag{7}$$

Figure 9 shows the magnification factor as a function of the damping ratio for our case. As it is apparent from the figure, smaller damping ratios result in larger magnification factors in the resonance region ($r = 1$). For the first four cases, we used the results of the measurements (compare figure 8(b)). Additionally, we calculated the magnification factor for cases with an even higher damping ratio. It is shown that a damping ratio ζ of 0.3 would already reduce the magnification factor below the value of 2. These results indicate that an increased damping results in a significantly smaller magnification factor reducing the oscillation amplitude for the resonance case.

3.3. Influence of ECDs on the ring spinning process

3.3.1. Single copper ring

As already mentioned, the stability of the rotating bearing is of great importance for the ring spinning process as the quality of the yarn will reduce drastically otherwise. Therefore, the influence of a single ECD on the process during the acceleration phase was tested as a first step. For this experiment, the PM ring was placed again at a distance of 4.5 mm from the superconductor during cool down to 77 K. Afterwards, the behavior of the bearing was characterized with and without a 1 mm thick copper ring between the superconductor and the PM ring. The

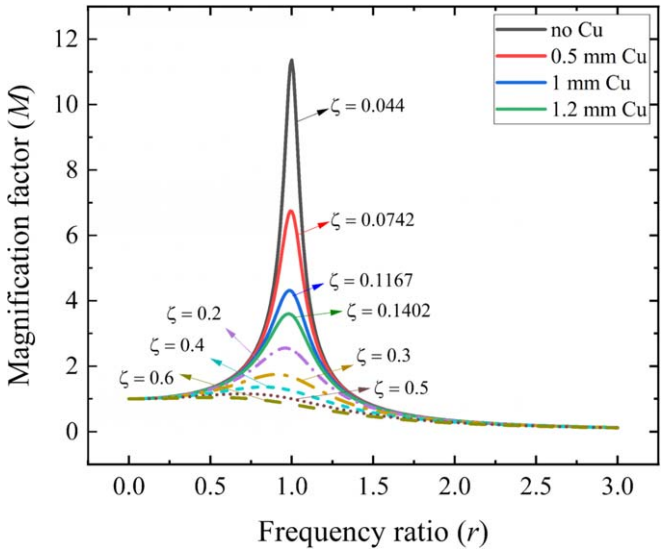

Figure 9. Magnification factor M as a function of the frequency ratio r for different damping ratios ζ. Solid lines are based on the damping ratios determined from impulse test measurements in section 3.1, whereas the broken lines are hypothetical cases with higher damping.

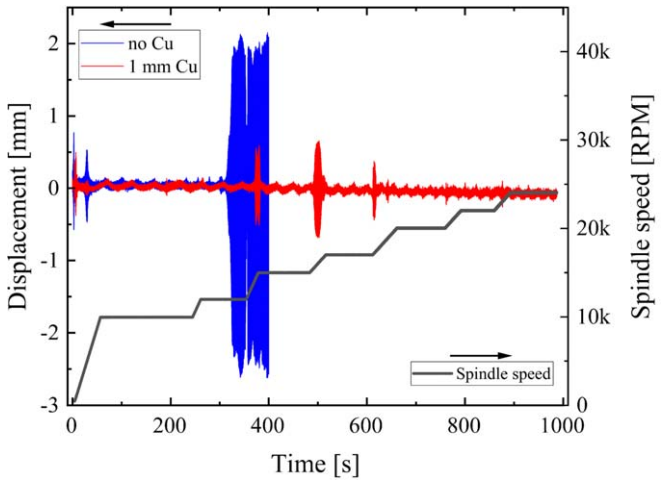

Figure 10. Radial displacement of the PM ring during the acceleration phase with and without a single 1 mm thick Cu ring (cooling height 4.5 mm, 77 K). The low-frequency oscillation of the measurement signal is due to the up-and-down movement of the ring rail leading to a continuous position change of the PM. Additionally, the spindle speed is shown for the case with the Cu ring; the PM ring's speed is slightly smaller.

gap between the PM ring and the cryostat surface of about 1.5 mm limits the maximum thickness of the ECD ring to 1 mm to ensure that no mechanical contact appears during high-speed rotation even for axial oscillations (compare amplitudes in figure 7(a)).

Figure 10 shows the displacement of the PM ring in radial direction during the acceleration phase for the setup with an additional ECD compared to the original measurement without any Cu ring. Whereas the displacement was too severe without an ECD to continue the acceleration above 12,000 RPM for safety reasons, these oscillations were significantly reduced with an additional 1 mm thick Cu plate so that the rotation speed could be increased further up to 24,000 RPM. But even in this case, resonances occur between 12,500–17,500 RPM, which might be triggered by an additional impulse input of the moving ring rail at its turning point. However, the amplitudes are smaller than in the original case and are damped away with increasing spindle speed. In summary, the yarn spinning process runs smoothly up to high speeds except for minor disturbances, which do not severely influence the yarn quality. Nevertheless, an even higher process stability is targeted, which might be achieved with a second Cu ring above the PM.

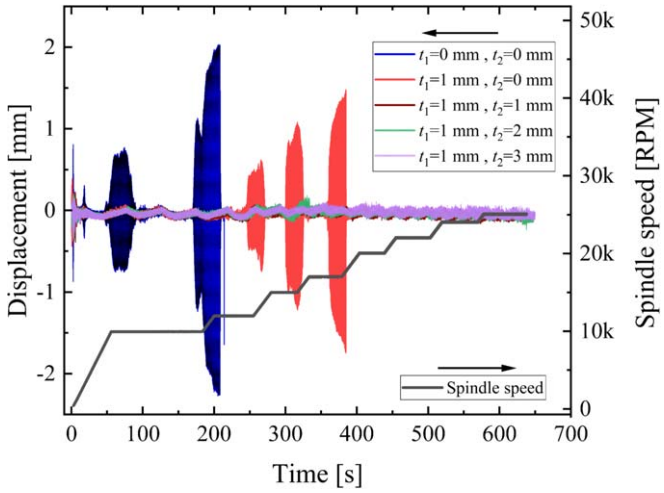

Figure 11. Radial displacement of the SMB during the acceleration phase with different ECD setups (cooling height 4.8 mm, T = 77 K). t_1 and t_2 are the lower and upper Cu ring thicknesses, respectively. Additionally, the spindle speed is shown. The speed of the PM ring is slightly smaller.

3.3.2. Two copper rings

To further increase the damping and to stabilize the ring spinning process, a new setup of the ECD was built, including copper rings below and above the PM. For simplicity, only 1 mm thick copper rings were fabricated, i.e., several rings will be piled up to increase the thickness of the upper ECD. Additionally, the field cooling height was increased to 4.8 mm for this set of experiments resulting in a reduced magnetic field in the superconductor, which lowers the interactive force between the superconductor and the PM, i.e., decreases the bearing stiffness. As a result, large oscillations of the PM ring were observed during acceleration without and even with a single 1 mm thick copper ring below the magnet (figure 11, blue and red signals). In both cases, the process was stopped due to safety measures. The lower stiffness of the bearing might explain the different behavior of the SMB for the case with a single copper ring compared to the previous measurement using cooling height of 4.5 mm. However, if a second copper ring is used above the PM, the oscillations are damped significantly stronger resulting in a smooth operation of the ring spinning process up to high speeds (compare figure 11). No significant changes were observed when the thickness of the upper ring is increased from 1 mm to 3 mm. The results indicate that eddy current dampers are effective passive devices for high-speed SMB applications.

3.4. Numerical modeling of the eddy current damper

3.4.1. Theoretical foundation

The detailed knowledge of the characteristic bearing properties, the magnetic field distribution of the PM, the geometrical distances between PM and superconductor, and the value of the Lorenz force arising from the damping elements might help us to design a suitable eddy current damper for specific configurations. Therefore, we created a numerical model to study the effect of these parameters on the dynamic properties, which helps to optimize a suitable ECD for the passive damping of vibrations. For that, a 3D numerical model was developed in COMSOL MULTIPHYSICS 5.6, which characterizes the dynamic behavior of the eddy current damper in relation to the PM ring. The numerical model was validated against the experimental results, which will be discussed in the next subsection. If we assume that the surface charge is neglected, the eddy current induced in the conductive plate moving with the velocity ν can be described as:

$$\vec{J} = \sigma(\vec{v} \times \vec{B}) \tag{8}$$

where σ is the conductivity of copper and B is the magnetic flux density of the PM ring. Biot-Savarts law can be applied to calculate the magnetic flux density in the space domain [35]. Here, we have to implement the constitutive relation for the magnetic field B using the remnant flux density $B_{r,}$ which was determined from the measured magnetic flux as discussed before in section 2.2:

$$\vec{B} = \mu_0 \mu_r \vec{H} + \vec{B}_r \tag{9}$$

Here, μ_0 is the permeability constant, μ_r the relative permeability of the Copper ring, H the magnetic field strength, and B_r the remnant flux density of the NdFeB PM ring. Sets of Maxwell's equations were solved to calculate numerically the induced flux density and current density inside the conductive plate as shown in equations (10) and (11)

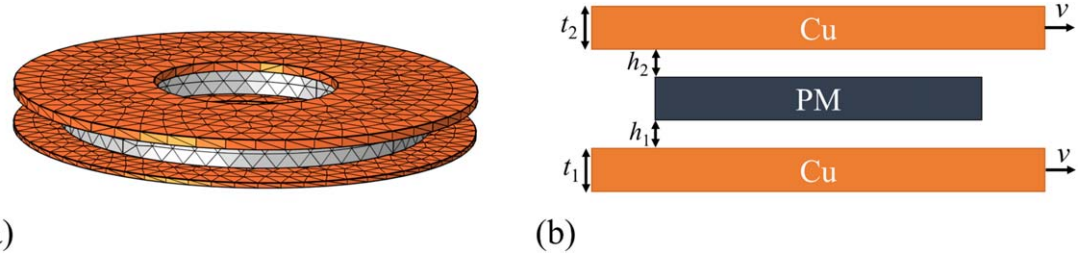

Figure 12. (a) Triangular structural mesh used in the FEM model (b) Schematic cross-sectional view of one half of the ECD setup.

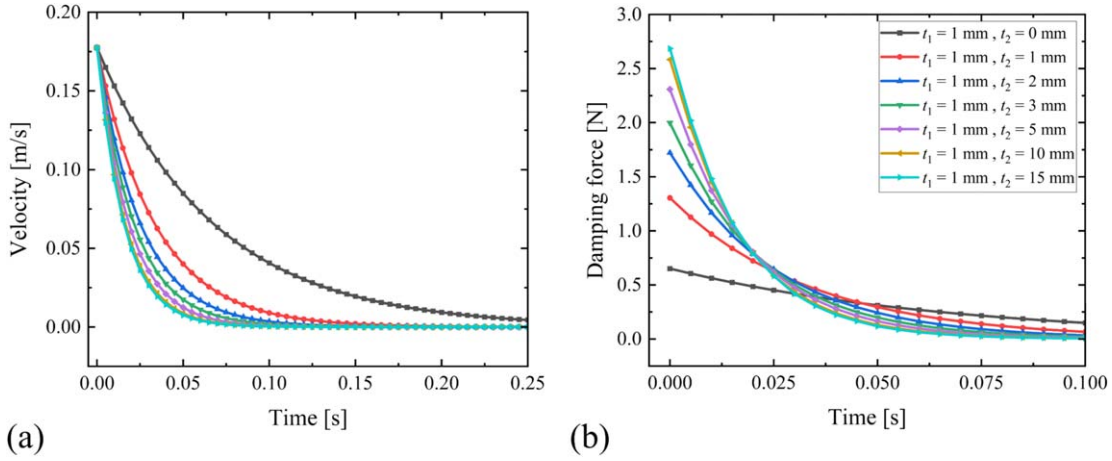

Figure 13. (a) Radial velocity of the magnet for different thicknesses t_2 of the upper copper ring; (b) Damping force applied to the bearing from the ECD elements.

$$\nabla \times (\mu^{-1}\nabla \times A) - \sigma v \times (\nabla \times A) + \sigma \nabla V = 0 \tag{10}$$

$$-\nabla \cdot (-\sigma v \times (\nabla \times A) + \sigma \nabla V) = 0 \tag{11}$$

where A is the magnetic vector potential and V the scalar electric potential. The Lorenz force, which is the interactive repulsive force generated between the PM ring and the conductive plate can be derived as follows:

$$F_l = \int_{Cu\ plate} (J \times B) dV \tag{12}$$

Here, the levitation force is calculated by integrating the cross-product of the induced current density and the magnetic flux over the volume of the conductive plate. To consider the lateral motion of the PM ring, the Lorenz force calculated above was coupled with Newton's first law $F = ma$, where the acceleration was reformulated as dv/dt:

$$\frac{dv}{dt} = \frac{F_l}{m} \tag{13}$$

with m as the mass of the PM ring. This equation was solved using a time-dependent ordinary differential equation (ODE) solver of the COMSOL software in parallel with the stationary solutions of Maxwell's equations described above. A triangular structured mesh was used for this purpose as shown in figure 12(a). The main geometrical parameters are included in the cross-section (see figure 12(b)).

In the simulations, the conductive plates were moved with respect to the PM using a one-directional displacement with an initial velocity. This procedure resulted in improved stability and convergence of the numerical model compared to the case of a moving magnet. However, the relative movement of the magnet with respect to the Cu rings remains similar to the experimental study. The maximal radial displacement velocity was determined from the data acquired by the laser sensor array for the magnet under resonance conditions to a value of $v_0 = 0.18\ \mathrm{m\ s^{-1}}$. All other geometrical and functional parameters used in the simulation are summarized in table 1.

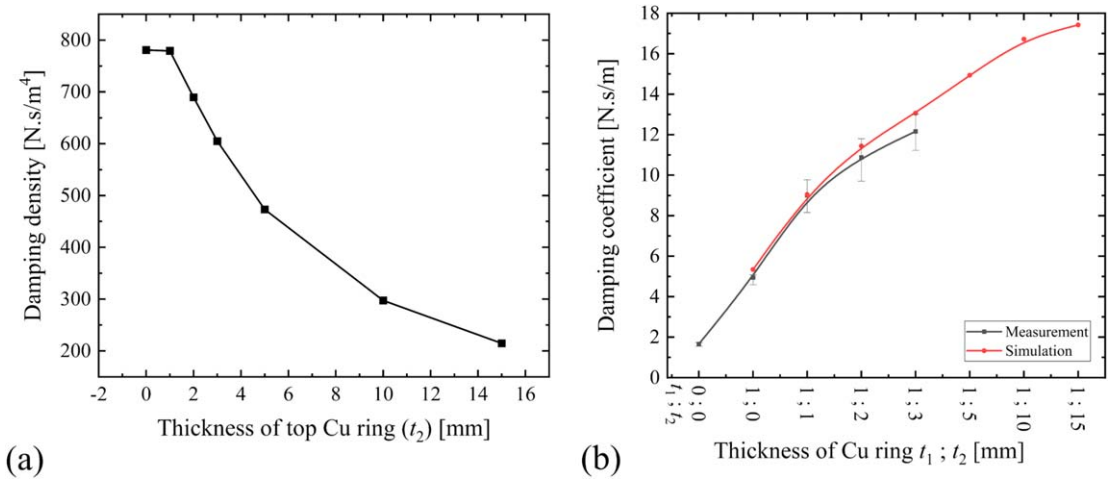

Figure 14. (a) Simulated damping density of the ECD setup in dependence of the upper copper ring thickness t_2 (b) Comparison of the simulated damping coefficient with measured data for the ECD setup.

Table 1. Geometrical and functional parameters used for simulation.

Parameter	Value [unit]	Description
t_1	1 [mm]	Thickness of the lower copper ring
t_2	0–15 [mm]	Thickness of the upper copper ring
h_1	0.5 [mm]	Air gap between lower copper ring and PM
h_2	0.5 [mm]	Air gap between upper copper ring and PM
v_0	0.18 [m/s]	Initial velocity
d_{in_Cu}	40 [mm]	Inner diameter of the copper ring
d_{out_Cu}	100 [mm]	Outer diameter of the copper ring
t_{PM}	6 [mm]	PM ring thickness
d_{in_PM}	50 [mm]	Inner diameter of the PM ring
d_{out_PM}	80 [mm]	Outer diameter of the PM ring
B_r	1.27 [T]	Remnant magnetic flux of the PM
m	0.25 [kg]	Mass of the PM
EC	$4.3 \cdot 10^7$ [S/m]	Electrical conductivity of copper according to the manufacturer

3.4.2. Results of the simulation

In the following, the ECD was modeled keeping the thickness of lower copper ring constant with $t_1 = 1$ mm, whereas the thickness of the upper copper ring (t_2) was varied from 0 to 15 mm. The air gap between the copper rings and the PM was kept constant at 0.5 mm on both sides to be consistent with the performed measurements. In figure 13, the velocity of the magnet and the Lorenz force are plotted against time for different Cu thicknesses. It is apparent that the velocity drops faster to zero, and the initial damping force gets larger as the thickness of the ECD increases. This is due to larger values of the induced current in the conductive ring leading to a larger magnetic field generated by these eddy currents.

In figure 14(a), the damping density, determined as the damping force per volume of the conductive Cu rings, is plotted versus the thickness of the upper copper ring. The damping density is a fine measure for evaluating the damping efficiency of the ECD. The first two cases show the highest density among all studied configurations, where one 1 mm Cu plate was underneath the PM ring, and either none or one 1 mm Cu plate was placed above. As the thickness of Cu increases, the damping density will decrease as a smaller relative volume of Cu will contribute to the damping of the PM ring.

Finally, the damping coefficient of the ECD setup was calculated by dividing the damping force by the velocity of the PM ring. It is shown in figure 14(b) (red curve) that the damping coefficient significantly increases with increasing Cu thickness. Whereas a value below 2 N·s/m is typically observed for the bearing without an ECD, an additional 1 mm thick Cu ring below the PM results already in a damping coefficient above 5 N·s/m.

This value further increases, when additional Cu rings are added above the magnet. To compare the damping coefficient calculated from the ECD model with the experimentally studied cases (compare section 3.3.2), the measured initial damping coefficient of the SMB system without any external damper and with the different Cu rings were added to the plot. Both results are summarized in figure 14(b). In general, a good agreement was found between the experimental values and the simulations for thin Cu plates. With increasing upper Cu thickness, the measured damping coefficients are smaller than the calculated ones. As mentioned in section 3.3.2, only 1 mm thick copper plates were used for the experimental studies, i.e., up to 3 rings were piled up to realize a larger Cu thickness. This might result in a different induced current flow, which can explain the deviation between the simulation and the measurement results for the 2 mm and 3 mm thick Cu rings placed above the PM. However, the difference between the simulations and the measurements are not severe, which indicates that the developed model might be used and modified for studying different ECD geometries as well as for the application of different materials in such dampers.

In summary, the described simulation model allows to estimate the damping coefficient for our particular SMB, when Cu rings with different thickness are added to the system. This knowledge allows to design a dynamically stable bearing even if an external vibration excites the bearing close to its resonance frequency. It was shown for a particular case in the ring spinning process in section 3.3.2. that already a Cu thickness of 1 mm below and above the PM ring can efficiently damp such detrimental oscillations occurring during the acceleration phase. Additional tests will be performed for different cooling conditions (i.e. temperature and cooling height) as well as at higher speeds to validate the simulation further.

4. Conclusion

The effect of eddy current damping elements was studied for a frictionless SMB twisting system designed to speed up the conventional ring spinning process in textile industry. The particular emphasis was on the passive damping of large amplitude oscillations of the PM in such a high-speed rotating SMB observed during the acceleration stage. The analysis of the PM movement during this stage by an array of laser distance sensors indicated that these oscillations originate from a resonance case, where an external driving force with frequencies close to the natural frequency of the SMB couples in the system. To avoid the detrimental effect of these oscillations, conductive copper rings were implemented below and above the PM ring to act as an eddy current damper by absorbing the energy of these oscillatory movements. Different arrangements and thicknesses of these copper rings were studied to find an optimal setup for such ECD elements for the ring spinning process. As a result, it was possible to eliminate the detrimental oscillations of the PM ring during acceleration by adding at least two copper rings with a thickness of 1 mm below and above the magnet. Simultaneously, a 3D numerical finite element model was developed using COMSOL MULTIPHYSICS 5.6 to study the eddy current damping in more detail and to calculate the damping coefficient for different configurations. It was shown that the damping coefficient increases significantly with the copper ring thickness. The simulations were in good agreement with the experimental results, so that the model might be further adjusted to optimize the design of the bearing for specific applications.

Acknowledgments

This work was supported by the Deutsche Forschungsgemeinschaft (DFG, German Research Foundation) through the joint project 459466327 (DFG CH 174/61-1, DFG BE 4791/5-1, and DFG HU 1726/9-1).

Data availability statement

All data that support the findings of this study are included within the article (and any supplementary files).

Declaration of interests

The authors declare that they have no known competing financial interests or personal relationships that could have appeared to influence the work reported in this paper.

ORCID iDs

M Baloochi https://orcid.org/0000-0002-8888-7237

T Espenhahn https://orcid.org/0000-0002-7621-8810
M Hossain https://orcid.org/0000-0003-2362-3449
Y Perez-Delgado https://orcid.org/0000-0001-6482-6272
R Hühne https://orcid.org/0000-0002-0030-6048

References

[1] Supreeth D K, Bekinal S I, Chandranna S R and Doddamani M 2022 A review of superconducting magnetic bearings and their application *IEEE Trans. Appl. Supercond.* **32** 3800215
[2] Moon F C and Chang P Z 1990 High-speed rotation of magnets on high Tc superconducting bearings *Appl. Phys. Lett.* **56** 397–9
[3] Hull J R 2000 Superconducting bearings *Supercond. Sci. Technol.* **13** R1
[4] Werfel F N *et al* 2012 Superconductor bearings, flywheels and transportation *Supercond. Sci. Technol.* **25** 014007
[5] Strasik M *et al* 2007 'Design, fabrication, and test of a 5-kWh/100-kW flywheel energy storage utilizing a high-temperature superconducting bearing *IEEE Trans. Appl. Supercond.* **17** 2133–7
[6] Werfel F N *et al* 2008 250 kW flywheel with HTS magnetic bearing for industrial use *J. Phys. Conf. Ser.* **97** 012206
[7] Strasik M *et al* 2010 An overview of Boeing flywheel energy storage systems with high-temperature superconducting bearings *Supercond. Sci. Technol.* **23** 034021
[8] Lin Q *et al* 2012 Research of radial high temperature superconducting magnetic bearings for cryogenic liquid pumps *IEEE Trans. Appl. Supercond.* **22** 5201604
[9] Kloeppel S *et al* 2017 Superconducting bearings for a LHe transfer pump *IOP Conf. Ser.: Mater. Sci. Eng.* **278** 012029
[10] Johnson B R *et al* 2017 A large-diameter hollow-shaft cryogenic motor based on a superconducting magnetic bearing for millimeter-wave polarimetry *Rev. Sci. Instrum.* **88** 105102
[11] Espenhahn T, Sparing M, Berger A, Nielsch K and Hühne R 2021 Dependency of hysteretic loss on speed and tilt in a rotating superconducting magnetic bearing *Supercond. Sci. Technol.* **34** 125004
[12] Sparing M *et al* 2020 Analysis of the high-speed rotary motion of a superconducting magnetic bearing during ring spinning *Eng. Res. Express* **2** 35039
[13] Espenhahn T, Sparing M, Niklas C, Nielsch K and Huhne R 2021 Dynamic characteristics of a superconducting magnetic bearing under μm displacements *IEEE Trans. Appl. Supercond.* **31** 5000105
[14] Sparing M *et al* 2015 Superconducting magnetic bearing as twist element in textile machines *IEEE Trans. Appl. Supercond.* **25** 25–8
[15] Hossain M *et al* 2014 Innovative twisting mechanism based on superconducting technology in a ring-spinning system *Text. Res. J.* **84** 871–80
[16] Sparing M *et al* 2016 Dynamics of rotating superconducting magnetic bearings in ring spinning *IEEE Trans. Appl. Supercond.* **26** 3–6
[17] Komori M and Shiraishi C 2003 A levitated motor with superconducting magnetic bearings assisted by self-sensing AMBs *IEEE Trans. Appl. Supercond.* **13** 2189–92
[18] Komori M, Matsuoka S and Fukata S 1996 Evaluations of a hybrid-type superconducting magnetic bearing system *IEEE Trans. Appl. Supercond.* **6** 178–82
[19] Miyagawa Y, Kameno H, Takahata R and Ueyama H 1999 A 0.5 kWh flywheel energy storage system using a high-T/sub c/ superconducting magnetic bearing *IEEE Trans. Appl. Supercond.* **9** 996–9
[20] Tang J, Wang K and Xiang B 2017 Stable control of high-speed rotor suspended by superconducting magnetic bearings and active magnetic bearings *IEEE Trans. Ind. Electron.* **64** 3319–28
[21] Yu J, Deng Z, Li H, Ma S, Zhao J and Wang L 2019 Vibration suppression of high-temperature superconducting maglev system via electromagnetic shunt damper *J. Supercond. Nov. Magn.* **32** 2819–28
[22] Yan B, Wang K, Hu Z, Wu C and Zhang X 2017 Shunt damping vibration control technology: a review *Appl. Sci.* **7** 494
[23] Sasaki M and Sugiura T 2016 Vibration reduction of rotor supported by superconducting magnetic bearing utilizing electromagnetic shunt damp *IEEE Trans. Appl. Supercond.* **26** 10–3
[24] Diez-Jimenez E, Rizzo R, Gómez-García M J and Corral-Abad E 2019 Review of passive electromagnetic devices for vibration damping and isolation *Shock Vib.* **2019** 1250707
[25] Zhang H Y, Chen Z Q, Hua X G, Huang Z W and Niu H W 2020 Design and dynamic characterization of a large-scale eddy current damper with enhanced performance for vibration control *Mech. Syst. Signal Process.* **145** 106879
[26] Ebrahimi B, Khamesee M B and Golnaraghi F 2009 Eddy current damper feasibility in automobile suspension: modeling, simulation and testing *Smart Mater. Struct.* **18** 015017
[27] Sodano H A, Bae J S, Inman D J and Keith Belvin W 2005 Concept and model of eddy current damper for vibration suppression of a beam *J. Sound Vib.* **288** 1177–96
[28] Bae J S, Kwak M K and Inman D J 2005 Vibration suppression of a cantilever beam using eddy current damper *J. Sound Vib.* **284** 805–24
[29] Gao H, Wang H, Li J, Mao J and Wang Z 2022 Dynamic behavior and damping enhancement of cable with negative stiffness inerter damper *Int. J. Mech. Sci.* **235** 107664
[30] Jiang Z F and Gou X F 2015 Eddy damping effect of additional conductors in superconducting levitation systems ' *Phys. C Supercond. its Appl.* **519** 112–7
[31] Jin L *et al* 2017 Effect of eddy current damper on the dynamic vibration characteristics of high-temperature superconducting maglev system *IEEE Trans. Appl. Supercond.* **27** 3601706
[32] Detoni J G, Cui Q, Amati N and Tonoli A 2016 Modeling and evaluation of damping coefficient of eddy current dampers in rotordynamic applications *J. Sound Vib.* **373** 52–65
[33] Hossain M *et al* 2020 *In situ* measurement of the dynamic yarn path in a turbo ring spinning process based on the superconducting magnetic bearing twisting system *Text. Res. J.* **90** 951–68
[34] Hossain M *et al* 2017 Mathematical modeling, simulation and validation of the dynamic yarn path in a superconducting magnet bearing (SMB) ring spinning system *Text. Res. J.* **87** 1011–22
[35] Bae J S, Hwang J H, Park J S and Kwag D G 2009 Modeling and experiments on eddy current damping caused by a permanent magnet in a conductive tube *J. Mech. Sci. Technol.* **23** 3024–35